音波のための高精度陰解法と、その自由表面流れ問題への応用

An Accurate Implicit Method for Equations of Sound and
its Application to Free-Surface Problems

井田真人，群馬大 SVB 研，〒376-8515 群馬県桐生市天神町 1－5－1, E-mail: ida@vbl.gunma-u.ac.jp
Masato Ida, SVBL, Gunma University, 1-5-1 Tenjin-cho, Kiryu-shi, Gunma 376-8515

We propose an implicit solver for the acoustic terms in the compressible Navier-Stokes equations by employing the concept used in the “extrapolation scheme”. The present scheme has temporally quasi-2nd-order accuracy in low CFL condition and smoothly transforms to the Poisson equation, used in the SMAC algorithm, in quite high CFL condition. Namely, this scheme has higher accuracy than the backward Euler scheme and is applicable to multiphase flow problems in which incompressible materials are involved. We demonstrate its accuracy and robustness with some examples of sound-wave propagation and multiphase flow problems by coupling this scheme with the hybrid interpolation-extrapolation scheme (Comput. Phys. Commun. **132**, 2000, p.44) for convection equation.

1. Introduction

In this paper we propose an improved numerical solver for the unified solution of compressible and incompressible fluids. The convection terms in the Euler equations of fluid flows are solved with the hybrid interpolation-extrapolation method proposed in Refs. 1–3 and the acoustic terms in the same equations are solved with a generalized Crank-Nicholson method which will be introduced in the following section. The accuracy and the robustness of the improved method are demonstrated with some linear and nonlinear test examples and finally an application to the bubble dynamics (the pulsation and the movement) in an acoustic field with the compressible Navier-Stokes equations is shown in Sec. 6.

2. Generalized Crank-Nicholson method for the acoustic terms

2. 1. A weighted formula

By eliminating the convection terms, the Euler equations are reduced to the following equations:

$$\frac{\partial \rho}{\partial t} = -\rho \nabla \cdot \mathbf{u}, \tag{1}$$

$$\frac{\partial \mathbf{u}}{\partial t} = -\frac{\nabla p}{\rho}, \tag{2}$$

$$\frac{\partial p}{\partial t} = -\rho C_S^2 \nabla \cdot \mathbf{u}, \tag{3}$$

where ρ, $\mathbf{u}$, p and C_S denote the density, the velocity vector, the pressure and the local sound speed, respectively. In this section we introduce an implicit solver for those equations.

In general, numerical solution with the backward Euler differencing such that used in the CUP method[(4)] tends to be diffusive because of its dissipation property due to truncation error. Here we try to reduce the dissipation by rewriting the CUP scheme into more general form. For simplicity, the following discussion is limited in 1D case for a while. Here we introduced a variable α and discretize Eqs. (1)–(3) with this as follows:

$$\frac{\rho^{n+1} - \rho^*}{\Delta t} = -\rho^* [\alpha u_x^{n+1} + (1-\alpha) u_x^*], \tag{4}$$

$$\frac{u^{n+1} - u^*}{\Delta t} = -\frac{1}{\rho^*} [\alpha p_x^{n+1} + (1-\alpha) p_x^*], \tag{5}$$

$$\frac{p^{n+1} - p^*}{\Delta t} = -\rho^* C_S^{*2} [\alpha u_x^{n+1} + (1-\alpha) u_x^*], \tag{6}$$

where n denotes the number of computational steps, the subscript x shows the derivation with x and the quantities with * shows that after solving the convection terms. Taking divergence of Eq. (5) and substituting it into Eq. (6) yield

$$\frac{p^{n+1} - p^*}{\Delta t} = \alpha \rho^* C_S^{*2} \Delta t \left[\frac{\alpha p_x^{n+1} + (1-\alpha) p_x^*}{\rho^*}\right]_x - \rho^* C_S^{*2} u_x^*. \tag{7}$$

Obviously this formula corresponds to the conventional pressure equation used in the CUP method for α = 1 and becomes a Crank-Nicholson like one for α = 0.5. By choosing α properly, higher resolution of solution than that with the backward Euler method may be expected.

For determining α, here we introduce a simple model. In the model, only three grid points, i = (–1, 0, 1), are contained and the pressure is fixed as p = 0 at its boundaries. By assuming α is locally constant, Eq. (7) is rewritten approximately as

$$\frac{p^{n+1} - p^*}{\Delta t} = \rho^* C_S^{*2} \Delta t \left[\alpha^2 \left(\frac{p_x^{n+1}}{\rho^*}\right)_x + \alpha(1-\alpha)\left(\frac{p_x^*}{\rho^*}\right)_x\right] - \rho^* C_S^{*2} u_x^*. \tag{8}$$

By neglecting the last term of (8) as

$$\frac{p^{n+1} - p^*}{\Delta t} = \rho^* C_S^{*2} \Delta t \left[\alpha^2 \left(\frac{p_x^{n+1}}{\rho^*}\right)_x + \alpha(1-\alpha)\left(\frac{p_x^*}{\rho^*}\right)_x\right] \tag{9}$$

and by adopting the second-order centered discretization to the RHS of (9), we get the following finite-difference equation at the center of the region:

$$\frac{p_0^{n+1} - p_0^*}{\Delta t} = -\left(\frac{1}{\rho^*_{1/2}} + \frac{1}{\rho^*_{-1/2}}\right) \rho^*_0 \frac{C_{S0}^{*2} \Delta t}{h^2} [\alpha^2 p_0^{n+1} + \alpha(1-\alpha) p_0^*]. \tag{10}$$

By rewriting this, we have

$$\frac{p_0^{n+1}}{p_0^*} = \frac{1 - A_0 \alpha (1-\alpha)}{1 + A_0 \alpha^2}, \tag{11}$$

$$A_0 \equiv \left(\frac{1}{\rho^*_{1/2}} + \frac{1}{\rho^*_{-1/2}} \right) \rho^*_0 \left(\frac{C^*_{S\,0} \Delta t}{h} \right)^2 . \tag{12}$$

On the other hand, by replacing the LHS of Eq. (10) with $\partial p_0 / \partial t$ and setting

$$p_0^{n+1} = p_0^* = p_0 ,$$

we get the following differential equation in terms of p_0.

$$\frac{\partial p_0}{\partial t} = -\alpha \frac{A_0}{\Delta t} p_0 .$$

By solving this, we get

$$\frac{p_0(t+\Delta t)}{p_0(t)} = \exp(-A_0 \alpha) . \tag{13}$$

By assuming that the above two amplification factors of Eqs. (11) and (13) are equal, the following relation equation is obtained.

$$\frac{1 - A_0 \alpha (1-\alpha)}{1 + A_0 \alpha^2} = \exp(-A_0 \alpha) . \tag{14}$$

In Fig. 1, we show the numerical solution of this equation. We see that

$$\lim_{A_0 \to +0} \alpha(A_0) = 1/2 ,$$
$$\lim_{A_0 \to \infty} \alpha(A_0) = 1$$

and α increases monotonically from 1/2 to 1 for $A_0 \in [0, \infty)$. The profile shown in the figure is fitted with some arbitrary function in the practical use.

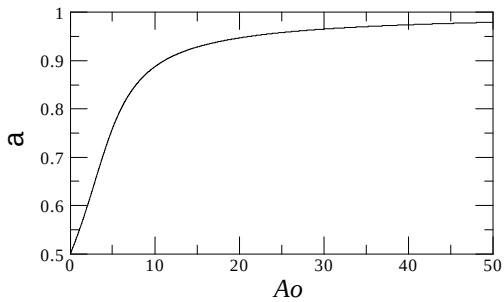

Fig. 1 Profile of the weighting factor respect to A_0.

In the above discussion, we adapted the basic concept used in the exponential scheme proposed by Patankar and Baliga (PB) for solving a heat-conduction equation[5]. However, the resulting weighting factor in the present scheme is different from theirs because we here treat equations in a different type. For the CUP scheme, Ito already led an exponential formula by using the concept directly[6], namely, the pressure equation used in the CUP method was treated as a heat-conduction equation with a source term and the resulting weighted formula is

$$\frac{p^{n+1} - p^*}{\Delta t} = \rho^* C_S^{*2} \Delta t [\alpha_{PB} \left(\frac{p_x^{n+1}}{\rho^*} \right)_x + (1-\alpha_{PB}) \left(\frac{p_x^*}{\rho^*} \right)_x] - \rho^* C_S^{*2} u_x^* .$$

The weighting factor Ito led is, thus, the same with Patankar and Baliga's one[5]:

$$\alpha_{PB}(A_0) = \frac{1}{1 - \exp(-A_0)} - \frac{1}{A_0} .$$

Here we point out an important difference in Ito's and the present formulas. For $A_0 \to +0$, both Ito's (PB's) and the present weighting factors converge to 1/2. In this case, the two formulas are reduced to

Ito's:

$$p^{n+1} = p^* - \rho^* C_S^{*2} u_x^* \Delta t + \frac{\rho^* C_S^{*2}}{2} \left(\frac{p_x^{n+1} + p_x^*}{\rho^*} \right)_x \Delta t^2 ,$$

and

Present:

$$p^{n+1} = p^* - \rho^* C_S^{*2} u_x^* \Delta t + \frac{\rho^* C_S^{*2}}{4} \left(\frac{p_x^{n+1} + p_x^*}{\rho^*} \right)_x \Delta t^2 .$$

By substituting $p^{n+1} = p^* + O(\Delta t)$ into the last term on the RHS of both equations, we get

Ito's:

$$p^{n+1} = p^* - \rho^* C_S^{*2} u_x^* \Delta t + \rho^* C_S^{*2} \left(\frac{p_x^*}{\rho^*} \right)_x \Delta t^2 ,$$

Present:

$$p^{n+1} = p^* - \rho^* C_S^{*2} u_x^* \Delta t + \frac{\rho^* C_S^{*2}}{2} \left(\frac{p_x^*}{\rho^*} \right)_x \Delta t^2 .$$

We see that the present one has temporally quasi-2nd-order accuracy, i.e., 2nd-order in time for $\partial(\rho^* C_S^{*2}) / \partial t \approx 0$ though Ito's one has only first-order in time and that the dominance of the diffusion term (the last term of both equations) in the present formula is weaker than that in Ito's one. From this, it should be expected that the present scheme provide less diffusive results than that with Ito's one.

Incidentally, when A_0 is approximated as

$$A_0 = \frac{\rho^*_0}{\rho^*_{1/2}} \left(\frac{C^*_{S\,0} \Delta t}{h} \right)^2 + \frac{\rho^*_0}{\rho^*_{-1/2}} \left(\frac{C^*_{S\,0} \Delta t}{h} \right)^2$$
$$\approx 2 \left(\frac{C^*_{S\,0} \Delta t}{h} \right)^2 = 2\lambda^2 ,$$

where

$$\lambda \equiv \frac{C^*_{S\,0} \Delta t}{h} ,$$

the weighting factor is regarded as a function in terms of the CFL number of sound. We should note here that the present scheme is applicable to incompressible-flow problems. Just same as the conventional pressure equation in the CUP method, the present one is reduced to that in the SMAC algorithm for infinite λ because, in this case, α converges to 1 and the present formula corresponds to the conventional one. As shown below, the simple Crank-Nicholson method with α fixed to 1/2 is not applicable to the incompressible flow problems. With α = 1/2 and infinite sound speed, the pressure equation (7) and Eq. (5) are reduced to

$$\left(\frac{p_x^{n+1}+p_x^*}{\rho^*}\right)_x = \frac{4u_x^*}{\Delta t}\ , \tag{15}$$

$$\frac{u^{n+1}-u^*}{\Delta t} = -\frac{p_x^{n+1}+p_x^*}{2\rho^*}\ . \tag{16}$$

By taking divergence of Eq. (16) and substituting Eq. (15) into it, we get

$$u_x^{n+1} = -u_x^*\ .$$

Obviously this does not satisfy the divergence-free flow condition.

For updating the velocity, we can use Eq. (5). For the density, we use

$$\rho^{n+1} = \rho^* + \frac{p^{n+1}-p^*}{C_S^{*2}}\ , \tag{17}$$

which is led from Eqs. (1) and (3) and corresponds to the conventional one.

We now extend the present formula into a two-dimensional one. For 2D case, we use

$$\frac{p^{n+1}-p^*}{\Delta t} = \rho^* C_S^{*2}\Delta t\,(\tilde{F}+\tilde{G}) - \rho^* C_S^{*2}\nabla\cdot\mathbf{u}^*\ , \tag{18}$$

where

$$\tilde{F} \equiv \alpha_1^2\left(\frac{p_x^{n+1}}{\rho^*}\right)_x + \alpha_1(1-\alpha_1)\left(\frac{p_x^*}{\rho^*}\right)_x\ ,$$

$$\tilde{G} \equiv \alpha_2^2\left(\frac{p_y^{n+1}}{\rho^*}\right)_y + \alpha_2(1-\alpha_2)\left(\frac{p_y^*}{\rho^*}\right)_y\ ,$$

and the parameters α_1 and α_2, which are for x and y direction, respectively, are determined with (14) and (12) as

$$\alpha_1(A1) = \alpha(A1)\ , \tag{19}$$

$$\alpha_2(A2) = \alpha(A2) \tag{20}$$

with

$$A1 \equiv \left(\frac{1}{\rho^*_{i+1/2,\,j}} + \frac{1}{\rho^*_{i-1/2,\,j}}\right)\rho^*_{i,\,j}\left(\frac{C^*_{S\,i,\,j}\Delta t}{h}\right)^2, \tag{21}$$

$$A2 \equiv \left(\frac{1}{\rho^*_{i,\,j+1/2}} + \frac{1}{\rho^*_{i,\,j-1/2}}\right)\rho^*_{i,\,j}\left(\frac{C^*_{S\,i,\,j}\Delta t}{h}\right)^2. \tag{22}$$

Same as the 1D case, this formula corresponds to the conventional one for $(\alpha_1, \alpha_2) = (1, 1)$ and becomes a quasi-2nd-order one for $(\alpha_1, \alpha_2) = (1/2, 1/2)$.

The use of the following alternative 2D formula which has only one parameter is not suitable.

$$\frac{p^{n+1}-p^*}{\Delta t} = \rho^* C_S^{*2}\Delta t\left[\alpha_3^2\nabla\cdot\left(\frac{\nabla p^{n+1}}{\rho^*}\right) + \alpha_3(1-\alpha_3)\nabla\cdot\left(\frac{\nabla p^*}{\rho^*}\right)\right]$$
$$-\rho^* C_S^{*2}\nabla\cdot\mathbf{u}^*.$$

With the same consideration used to get the parameter for 1D formula, the parameter α_3 is determined as

$$\alpha_3(A3) = \alpha(A3)$$

where

$$A3 = A1 + A2\ .$$

We see that $A3 > A1$ and $A3 > A2$ always and the formula is not reduced to the 1D one even when $\partial/\partial y = 0$ or $\partial/\partial x = 0$. Thus, we recommend the use of the former formula shown in Eq. (18).

2. 2. A multi-step solution technique

Compared with the conventional pressure equation, the present one needs larger computational effort to solve because there exists the parameters and second-order explicit terms. In this subsection, we introduce a scheme for reducing the additional effort by employing a multi-step solution technique.

Here we introduce a variable δp defined as

$$\delta p \equiv p^{n+1} - p^*\ . \tag{23}$$

By substituting this into Eq. (18) and vanishing p^{n+1}, we get

$$\frac{\delta p}{\Delta t} = \rho^* C_S^{*2}\Delta t\left[\alpha_1^2\left(\frac{\delta p_x}{\rho^*}\right)_x + \alpha_2^2\left(\frac{\delta p_y}{\rho^*}\right)_y\right]$$
$$+\rho^* C_S^{*2}\Delta t\left[\alpha_1\left(\frac{p_x^*}{\rho^*}\right)_x + \alpha_2\left(\frac{p_y^*}{\rho^*}\right)_y\right] - \rho^* C_S^{*2}\nabla\cdot\mathbf{u}^*. \tag{24}$$

With definitions of

$$\bar{u} \equiv u^* - \frac{p_x^*}{\rho^*}\Delta t, \tag{25}$$

$$\bar{v} \equiv v^* - \frac{p_y^*}{\rho^*}\Delta t, \tag{26}$$

Eq. (24) is rewritten as follows:

$$\frac{\delta p}{\Delta t} = \rho^* C_S^{*2}\Delta t\left[\alpha_1^2\left(\frac{\delta p_x}{\rho^*}\right)_x + \alpha_2^2\left(\frac{\delta p_y}{\rho^*}\right)_y\right]$$
$$-\rho^* C_S^{*2}\left[\alpha_1\bar{u}_x + \alpha_2\bar{v}_y + (1-\alpha_1)u_x^* + (1-\alpha_2)v_y^*\right]. \tag{27}$$

Equations (25) and (26) show an explicit solution of Eq. (2) and the terms on the RHS of (27) except for the first one can be determined explicitly. In Eq. (27), the explicit second-order term shown in Eq. (24) is vanished. While Yoon and Yabe have tried to adopt a multi-step solution technique to the conventional CUP scheme[7], noticeable reduction of computational effort and computational complexity by adapting the technique was not shown. Therefore we claim that the use of the multi-step technique is effective for the present scheme rather than the conventional one.

With the weighting parameters given in the previous section, Eq. (5) in terms of the velocity is extended to a two-dimensional one:

$$\frac{u^{n+1}-u^*}{\Delta t} = -\frac{\alpha_1 p_x^{n+1} + (1-\alpha_1)p_x^*}{\rho^*}, \tag{28}$$

$$\frac{v^{n+1}-v^*}{\Delta t} = -\frac{\alpha_2 p_y^{n+1} + (1-\alpha_2)p_y^*}{\rho^*}. \tag{29}$$

From those equations and definitions of (23), (25) and (26), we get the following equations:

$$u^{n+1} = \bar{u} - \alpha_1\frac{\delta p_x}{\rho^*}\Delta t, \tag{30}$$

$$v^{n+1} = \bar{v} - \alpha 2 \frac{\delta p_y}{\rho^*} \Delta t. \tag{31}$$

Those equations can be solved explicitly after solving the pressure equation.

Same as the 1D case, the density is updated with

$$\rho^{n+1} = \rho^* + \frac{\delta p}{C_S^{*2}}, \tag{32}$$

which corresponds to the conventional one used in the CUP method.

The 2D multi-step procedure introduced in this subsection is summarized as follows:

1. Calculate $\bar{\mathbf{u}}$ with Eqs. (25) and (26).
2. Calculate δp with Eq. (27).
3. Update $\bar{\mathbf{u}}$ to $\mathbf{u}^{n+1}$ with Eqs. (30) and (31).
4. Update ρ^* to ρ^{n+1} with Eq. (32).
5. Update p^* to p^{n+1} with $p^{n+1} = p^* + \delta p$.

The generalized Crank-Nicholson formula and the multi-step solution technique discussed in this section may be able to extend to a 3D one by using three weighting factors.

3. Averaging at phase boundary

For discretizing the acoustic terms on the staggered grids, we need to estimate the density at the velocity positions. In this section, we discuss how to estimate it. As discussed in Ref 1, the fluid interface is recognized with the zero level set of the level set function, ϕ, and materials are identified with the sigh of the function. Because, in our study, the level set function has a non-zero value at each grids, we need not consider the case $\phi_{i,j} = 0$[1, 3]. For example, if $\phi_{i+1,j} \cdot \phi_{i,j} < 0$, it is recognized that there exists an interface between $(x_{i+1,j}, y_{i+1,j})$ and $(x_{i,j}, y_{i,j})$. By using this function, we estimate the density at the velocity positions by a VOF like approach.

The use of the simple average (the half of sum) is not sufficient for the estimation because the phase information of the interface, which is described with the level set function, is not taken account into the discretization. Let us consider, for example, a case where an interface exists in segment $(x_{i+1,j}, y_{i+1,j})$–$(x_{i,j}, y_{i,j})$. In this case, if the simple average is used, the density at the center point is uniquely determined as $\rho_{i+1/2,j} = (\rho_{i+1,j} + \rho_{i,j})/2$ wherever the interface locates in the segment. Resultantly the phase information of which the level set function has is shut off from the underling scheme. Thus, we choose the VOF like approach.

We use the following averaging scheme:

$$\rho^*_{i+1/2,j} = \frac{|\phi^{n+1}_{i+1,j}|\rho^*_{i+1,j} + |\phi^{n+1}_{i,j}|\rho^*_{i,j}}{|\phi^{n+1}_{i+1,j}| + |\phi^{n+1}_{i,j}|} \quad \textit{for } \phi^{n+1}_{i+1,j}\phi^{n+1}_{i,j} < 0, \tag{33}$$

$$\rho^*_{i,j+1/2} = \frac{|\phi^{n+1}_{i,j+1}|\rho^*_{i,j+1} + |\phi^{n+1}_{i,j}|\rho^*_{i,j}}{|\phi^{n+1}_{i,j+1}| + |\phi^{n+1}_{i,j}|} \quad \textit{for } \phi^{n+1}_{i,j+1}\phi^{n+1}_{i,j} < 0 \tag{34}$$

where ϕ^{n+1} (= ϕ^*. Note that the interface location is fixed during the acoustic process) is the level set function after solving the convection part and we assume that the grid spacing is uniform. Those equations show the weighted average of the density with the absolute value of ϕ, i.e., it is assumed that the spatial profile of ϕ is piecewise linear. For the regions where the interface dose not across, we use the simple average like

$$\rho^*_{i+1/2,j} = \frac{\rho^*_{i+1,j} + \rho^*_{i,j}}{2},$$

$$\rho^*_{i,j+1/2} = \frac{\rho^*_{i,j+1} + \rho^*_{i,j}}{2}$$

as frequently done in the conventional CIP algorithm[8] or others.

The above averaging scheme can be used also for estimating other values at the velocity positions, i.e., the parameters led in Sec. 2.1, the diffusion coefficient in viscous-flow case and so on.

4. Stabilization of the derivative advancement

At the phase boundary it is not suitable to use the conventional schemes for updating the spatial derivatives[8–10] especially in the case where some materials of quite different properties are treated simultaneously. In general, the derivatives of the physical quantities are discontinuous at the phase boundaries. Let us consider, for example, a pressure distribution around phase boundary between two different incompressible fluids. For an incompressible fluid flow, the pressure is described with a Poisson equation:

$$\nabla \cdot \frac{\nabla p}{\rho} = 0.$$

This shows that, when the density is discontinuous, the pressure gradient is also discontinuous. When materials of great difference in compressibility are located side by side, it is expected that more complex and troublesome problem should be appeared. From such reasons, we claim that the advancement of the derivatives should be treated with care much more.

Here we recall the extrapolation concept discussed in Refs. 1–3. As pointed out in the papers, interpolation or differencing across the phase boundary is not physically valid and it causes serious numerical error. Therefore, the adaptation of extrapolation is suitable in such a region. Thus, in this section, we modify the conventional schemes by adapting the extrapolation concept.

The conventional scheme for $\partial_x f$ can be rewritten as

$$\partial_x f^{n+1}_{i,j} - \partial_x f^*_{i,j} = \frac{1}{2}\left(\frac{d_{i+1,j} - d_{i,j}}{h} + \frac{d_{i,j} - d_{i-1,j}}{h}\right), \tag{35}$$

$$d_{i,j} \equiv f^{n+1}_{i,j} - f^*_{i,j}.$$

We here introduce a switching parameter H, which is defined as

$$H_{i+1/2,j} = \begin{cases} 1 & \phi^{n+1}_{i+1,j}\phi^{n+1}_{i,j} > 0 \\ 0 & \textit{otherwise} \end{cases}, \tag{36}$$

$$H_{i,j+1/2} = \begin{cases} 1 & \phi^{n+1}_{i,j+1}\phi^{n+1}_{i,j} > 0 \\ 0 & \textit{otherwise} \end{cases}, \tag{37}$$

and modify Eq. (35) with this as follows:

$$\partial_x f^{n+1}_{i,j} - \partial_x f^*_{i,j} = \frac{1}{2}\left(H_{i+1/2,j}\frac{d_{i+1,j} - d_{i,j}}{h} + H_{i-1/2,j}\frac{d_{i,j} - d_{i-1,j}}{h}\right). \tag{38}$$

With this modification, the derivative $(d_{i+1,j} - d_{i,j})/h$ between $x_{i+1,j}$ and $x_{i,j}$ is vanished for $\phi^{n+1}_{i+1,j} \cdot \phi^{n+1}_{i,j} < 0$ and the advancement is done only with the values of an identical material. The conventional scheme for $\partial_y f$ can be modified with the same manner as

$$\partial_y f_{i,j}^{n+1} - \partial_y f_{i,j}^{*} = \frac{1}{2}\left(H_{i,j+1/2}\frac{d_{i,j+1}-d_{i,j}}{h} + H_{i,j-1/2}\frac{d_{i,j}-d_{i,j-1}}{h} \right). \tag{39}$$

Next, we modify the scheme for the cross derivative[10]. The conventional equation can be rewritten as

$$\begin{aligned}\partial_{xy} f_{i,j}^{n+1} - \partial_{xy} f_{i,j}^{*} = \frac{1}{4h^2}[&(d_{i+1,j+1}-d_{i,j}) - (d_{i-1,j+1}-d_{i,j}) \\ &-(d_{i+1,j-1}-d_{i,j}) + (d_{i-1,j-1}-d_{i,j})].\end{aligned} \tag{40}$$

We modify this as

$$\begin{aligned}&\partial_{xy} f_{i,j}^{n+1} - \partial_{xy} f_{i,j}^{*} \\ &= \frac{1}{4h^2}[H_{i+1/2,j+1/2}(d_{i+1,j+1}-d_{i,j}) - H_{i-1/2,j+1/2}(d_{i-1,j+1}-d_{i,j}) \\ &- H_{i+1/2,j-1/2}(d_{i+1,j-1}-d_{i,j}) + H_{i-1/2,j-1/2}(d_{i-1,j-1}-d_{i,j})]\end{aligned} \tag{41}$$

where

$$H_{i\pm1/2,j\pm1/2} = \begin{cases} 1 & \rho_{i\pm1,j\pm1}^{n+1}\rho_{i,j}^{n+1} > 0 \\ 0 & \textit{otherwise.} \end{cases} \tag{42}$$

This modification means that an extrapolation of $d_{i\pm1,j\pm1} = d_{i,j}$ is applied for $\rho_{i\pm1,j\pm1}^{n+1}\rho_{i,j}^{n+1} < 0$. With this modification, the advancement of the cross derivative is done only with the values of an identical material.

Though the extrapolations used above are merely rough compared with that used to solve the convection part[1–3], they may be sufficient because they are applied only to the derivatives which may need only a less accuracy than the quantities.

5. Numerical tests

In this section, we conduct some numerical tests for demonstrating the effectiveness of the improvements introduced in the previous subsections. Because it is obvious that, in a high-CFL condition, the present scheme for the pressure equation be almost equivalent to the existing ones (Yabe-Wang's and Ito's), we mainly show results in low-CFL conditions.

Example 5. 1.

First, we introduce some results of a one-dimensional linear problem. By setting $\rho = 1$ and $C_S = 1$, Eqs. (1)–(3) in one spatial dimension are reduced to a system of linear partial differential equations as

$$\frac{\partial u}{\partial t} = -\frac{\partial p}{\partial x}, \quad \frac{\partial p}{\partial t} = -\frac{\partial u}{\partial x}.$$

As well known, this system can be rewritten into linear wave equations with the constant propagation velocity.

Figure 2 shows results of this system obtained with the present and the conventional schemes with an initial condition:

$$u(x,0) = 0, \quad p(x,0) = 1,$$
$$x \in [0,400]$$

and a boundary condition:

$$p(0,t) = 1,$$
$$p(400,t) = 1 + 0.12(1 - \cos\omega_0 t)$$

where the angular frequency ω_0 is determined so that the wavelength of the sound wave emitting from the right-side boundary is to be 25. The grid spacing h is uniform and is set as h = 1. The results shown in Fig. 2 are at n = 1500 with a low CFL number (CFL = 0.25). Theoretically, the emitting sound wave should propagate with the constant speed without any dissipation. However, the results with Yabe-Wang's and Ito's schemes are diffusive although the CFL number is low. While the result with Ito's one is better than that with Yabe-Wang's, it is obviously less accurate than that with the present one. In the result with the present scheme, any noticeable error cannot be seen except at the front of the wave where a large curvature exists in the waveform.

From the above results, we know that, in small-CFL condition, the present scheme provides less diffusive results than that with Yabe-Wang's and Ito's ones.

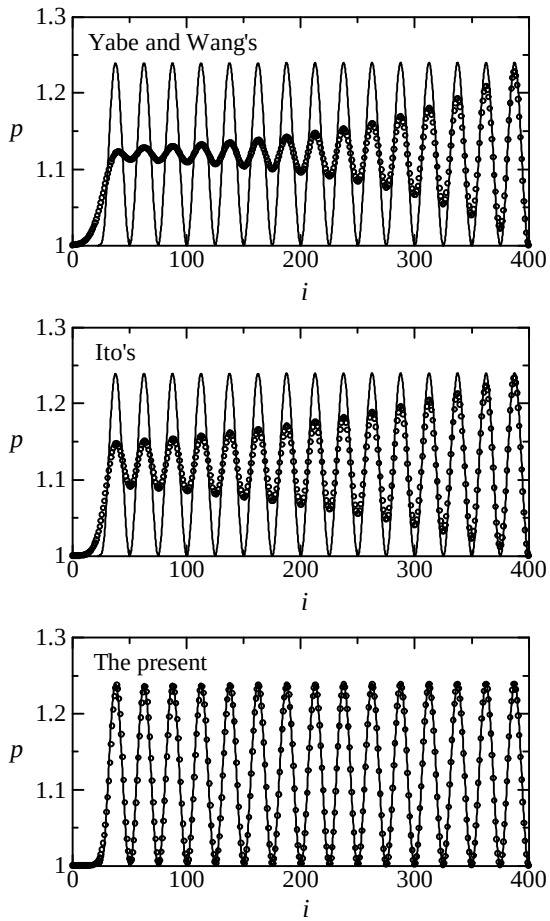

Fig.2 Linear propagation of sinusoidal sound wave. The solid line and the dots denote the theoretical and the numerical results, respectively.

Example 5. 2.

Next, we solve a one-dimensional nonlinear problem. We show results with an initial condition:

$$\rho(x,\ 0) = \begin{cases} 1 & \textit{for } x < 0, \\ 1.025\times10^{-3} & \textit{elsewhere}, \end{cases}$$
$$u(x,\ 0) = 0, \quad p(x,0) = 1, \quad x \in [-1.6, 0.4]$$

and a boundary condition:

$$\begin{cases} p(-1.6, t) = 1, \\ p(0.4, t) = 1 + 0.12(1 - \cos \omega_1 t) \end{cases}$$

where the angular frequency ω_1 is determined so that the wavelength of the emitting sound wave be $20h$ and 200 grid points are used in the computational domain, namely h = 1/100. The sound speed is determined with

$$C_S^2 = \begin{cases} \dfrac{7(p + 3172.04)}{\rho} & \textit{for } x < 0, \\ \dfrac{1.4p}{\rho} & \textit{elsewhere.} \end{cases}$$

We choose $\Delta t = 4 \times 10^{-5}$ and, in this case, the CFL number is about 0.6 in $x < 0$ and about 0.15 elsewhere. The level set function is set as a color function like

$$\phi = \begin{cases} 1 & \textit{for } x < 0, \\ -1 & \textit{elsewhere.} \end{cases}$$

In Fig. 3, we show pressure distributions of this example at n = 530. At the interface, the emitting sound wave transmits and reflects. On the left side of the interface, we can see a transmitting wave which has larger amplitude and longer wavelength than that of the emitting wave. On the contrary, on the right side, we can see that an interference of the reflecting and the emitting wave occurs. Just same as the previous ones, the results with the existing schemes are diffusive and the amplitudes of the transmitting and reflected waves are estimated smaller than the correct one.

With this example, we now compare the conventional and the modified schemes for the derivative advancement, which was discussed in Sec. 4. Here the quantities are updated with the present scheme. Figure 4 shows the density gradient ρ_x updated with the present and the conventional schemes up to n = 440. The result with the present one is stable and smooth, while that with the conventional one has strong overshoots around the interface. When such an unstable profile of the gradient is used in the convection process where the cubic and quasi-quadratic Hermite interpolation is done[1–3], numerical instability or numerical dispersion might be appeared around the interface. This result might prove the validity of the present scheme.

6. Application to the bubble dynamics in an acoustic field

In this section we show application results to the bubble dynamics in an acoustic field. Here we use the compressible Navier-Stokes equations with the surface-tension term as the governing equation[11]. The convection terms in the equation are solved with the hybrid interpolation-extrapolation method and the acoustic terms are solved with the generalized Crank-Nicholson method. The CSF model[12] is adapted to the surface-tension term and the conventional 2nd-order centered differencing is to the viscous terms.

In this problem, there exist some interesting features in the view of numerical simulation such as the existence of the interface where the density and the sound speed are highly jumped and the compressibility of the bubble being not negligible. Furthermore, for the dynamics of micro bubbles like used in the experiment of sonoluminescence[13] and the medical applications[14], the viscous effect is not negligible. In the boundary integration method[15, 16] which has been used to simulate multi-bubble dynamics, inviscid irrotational flow is assumed and, thus, the method is not applicable to the micro-bubble problems.

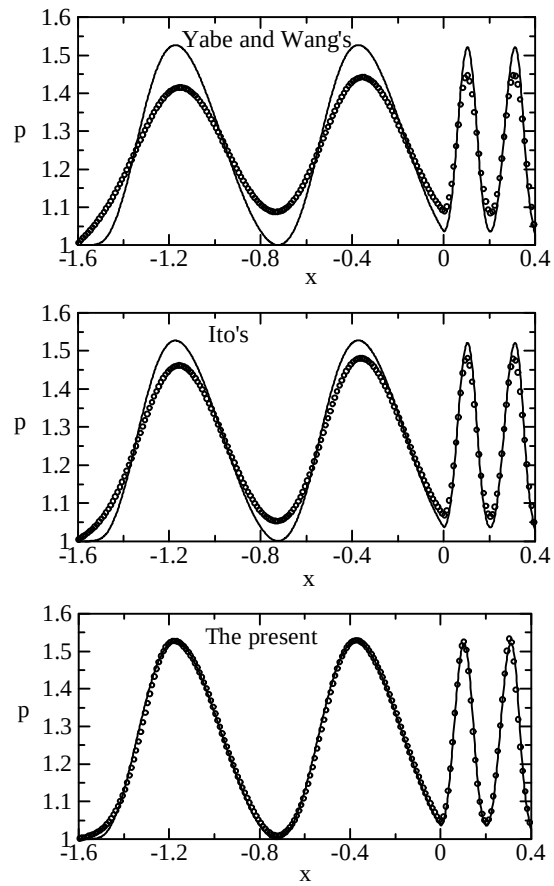

Fig. 3 Propagation of sound wave in a composite material. The solid line and the dots denote the numerical results with 200 and 800 numbers of grids, respectively.

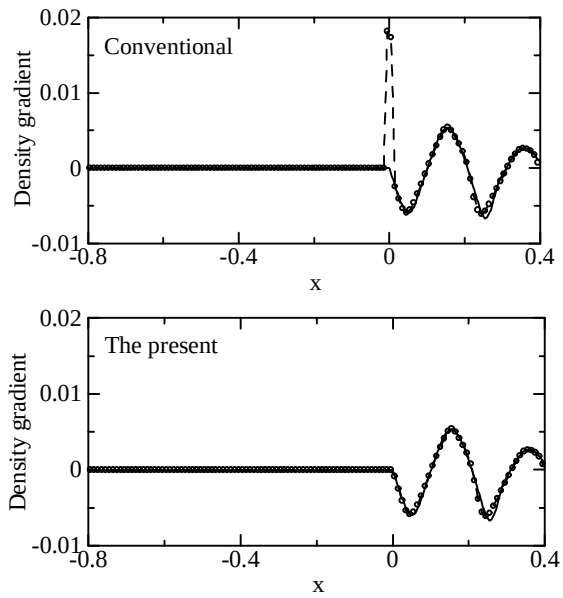

Fig. 4 The density gradient at n = 440. The solid line and the dots denote the numerical results with the 200 and 800 numbers of grids, respectively. In the result with the conventional scheme, strong overshoot can be seen at the interface.

Here we show a result of two-bubble case. We select axisymmetric coordinate (r, z) and use (100×250) number of uniform grids with $\Delta r = \Delta z$ =(1.5/20)μm. Initially the mass center of the left-side and the right-side bubbles, whose radius is 1.5μm,

are located at (r, z) = (0μm, –3μm) and (0μm, 3μm), respectively. The bubbles are filled with air with $\mu = 1.78 \times 10^{-5}$Pa s, where μ is the viscosity coefficient, and the surrounding medium is water with $\mu = 1.137 \times 10^{-3}$Pa s and their equilibrium densities are 1.226kg/m^3 and 1000kg/m^3. Equation of state for determining the sound speed in Eq. (3) is, for the gas phase, that for ideal gas with $\gamma = 1.33$, where γ is the specific heat ratio, and, for the liquid phase, is the Tait equation. The static pressure of the surrounding medium, p_0, is 101.3kPa and we use $\sigma = 7.28 \times 10^{-2}$Pa m, where σ is the surface-tension coefficient. The ultrasound with frequency f_{us} and amplitude p_{us} is applied as a boundary condition to the pressure. We use $f_{us} = 0.9 f_0$ and $p_{us} = 0.4 p_0$ in this example where f_0 ($\simeq$ 2.8MHz) is the eigenfrequency of the bubble.

Figure 5 (see the last page) shows the density and the pressure at the selected times. In the figure, not only the pulsation, the attraction of the bubbles due to the secondary Bjerknes force[17, 18] and the coalescence of them as a result of the attraction are observed. In Fig. 6, we show the temporal profile of the mean radius and the location of the left bubble with the sound amplitude until the coalescence occurs. In this figure, we can see that the bubble is strongly accelerated toward the other during its volume becomes large and is weekly repulsed during its volume becomes small. This behavior of bubbles agrees well with the theoretical interpretation of the secondary Bjerknes force.

During the computation shown above, the density jump at the phase boundary is resolved with no dissipation across the interface. This is achieved by the hybrid interpolation-extrapolation method for the convection terms.

7. Conclusions

In this paper we proposed an implicit numerical solver for the acoustic terms in the Euler equation of fluid flows and constructed an Eulerian solver for the multi-bubble dynamics by coupling it with the hybrid interpolation-extrapolation method and the CSF model. As shown in this paper and Ref. 11, this method provides more accurate result than that with the conventional CIP-CUP procedure and has sufficient accuracy for the direct simulation of pulsating and mutually interacting compressible bubbles in an acoustic field.

References

(1) M. Ida, Comput. Phys. Commun. **132** (2000) 44.
(2) M. Ida, in: Proc. 10th Symp. on Comput. Fluid. Dynam., Tokyo, Japan, 1996, p. 382 (in Japanese).
(3) M. Ida, Ph. D thesis, Tokyo Institute of Technology, 1998 (unpublished).
(4) T. Yabe and P. Y. Wang, J. Phys. Soc. Japan **60** (1991) 2105.
(5) S. V. Patankar and B. R. Baliga, Numerical Heat Transfer **1** (1978) 27
(6) S. Ito, in: Proc. The 43rd Nat. Cong. of Theoretical & Applied Mechanics, 1994, p. 311 (in Japanese).
(7) S. Y. Yoon and T. Yabe, Comput. Phys. Commun. **119** (1999) 149.
(8) T. Yabe and T. Aoki, Comput. Phys. Commun. **66** (1991) 219.
(9) H. Takewaki and T. Yabe, J. Comput. Phys. **70** (1987) 355.
(10) T. Aoki, Comput. Fluid Dynam. J. **4** (1995) 279.
(11) M. Ida and Y. Yamakoshi, (submitted).
(12) J. U. Brackbill, D. B. Kothe and C. Zemach, J. Comput. Phys. **100** (1992) 335.
(13) K. Yasui: Phys. Rev. lett. **83** (1999) 4297.
(14) P. A. Dayton et al: IEEE Trans. Ultrason. Ferroelect. & Freq. Control **44** (1997) 1264.
(15) J. R. Blake, B. B. Taib and G. Doherty: J. Fluid Mech. **170** (1986) 479.
(16) N. A. Pelekasis and J. A. Tsamopoulos: J. Fluid Mech. **254** (1993) 501.
(17) L. A. Crum: J. Acoust. Soc. Am. **57** (1975) 1363.
(18) A. Prosperetti: Ultrasonics **22** (1984) 115. (and references therein)

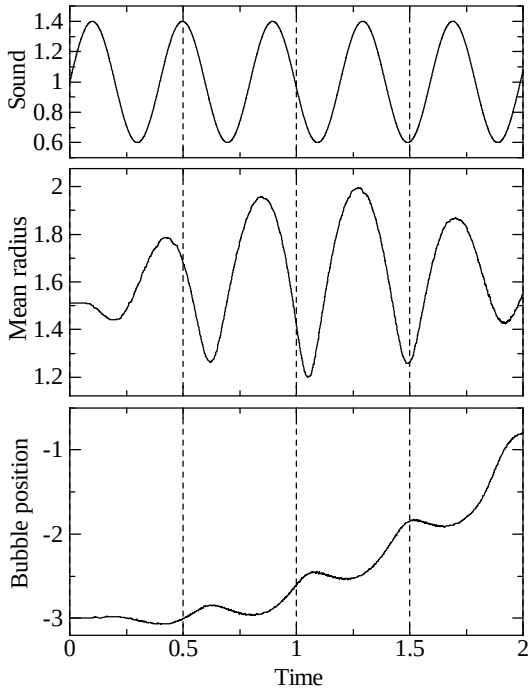

Fig. 6 Temporal profile of the mean radius (middle) and the position (lower) of the left bubble with the sound (upper).

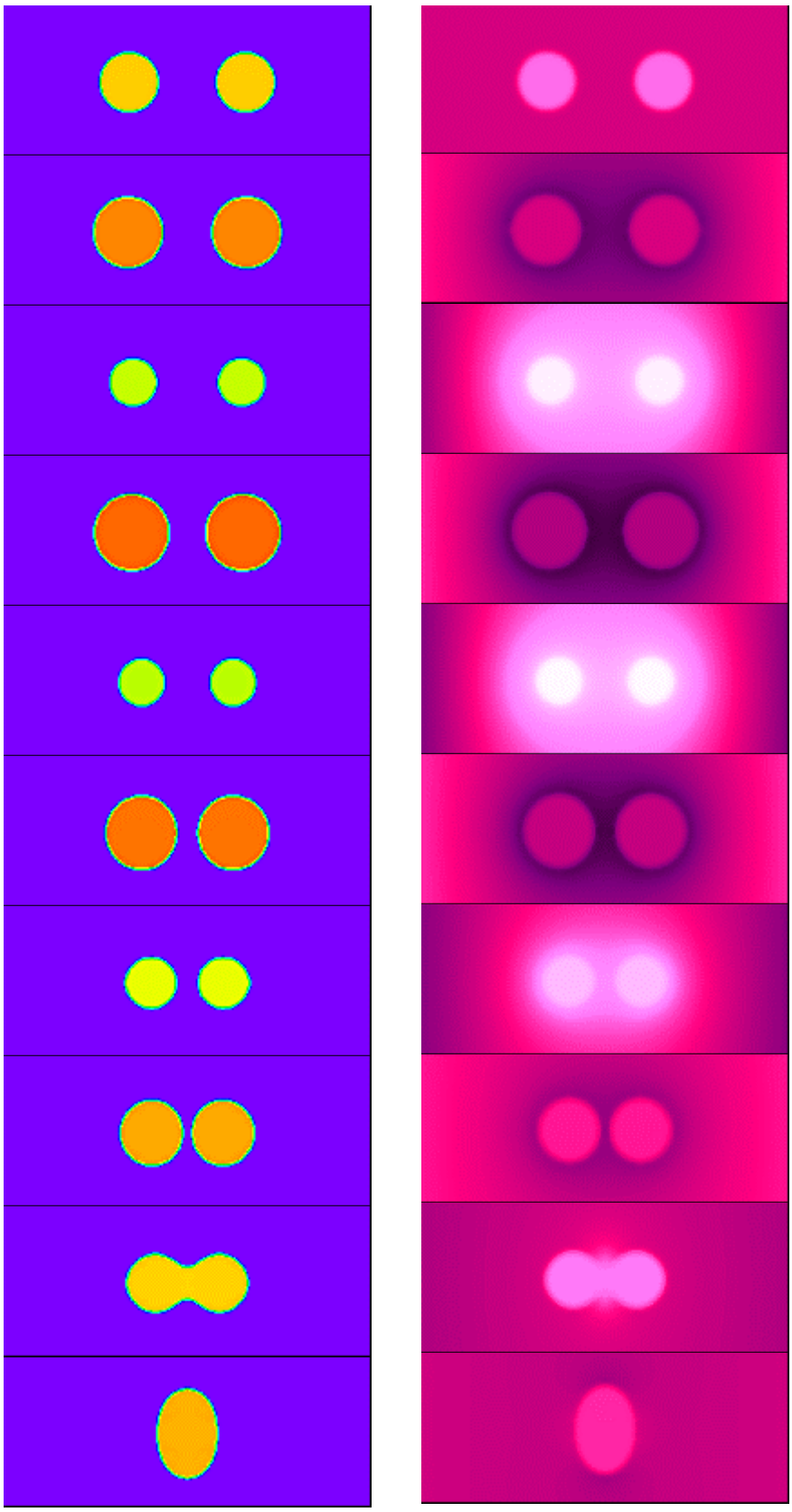

Fig. 5 Mutual interaction of two bubbles in an acoustic field. The left column is the density and the right one is the pressure. The time sequence is upper to lower and the plotted times are 0, 0.42, 0.62, 0.84, 1.04, 1.28, 1.48, 1.7, 1.82, 2.12μs. The coalescence occurs at about 1.8μm.